HHS Public Access

Author manuscript

FEBS Lett. Author manuscript; available in PMC 2018 May 01.

Published in final edited form as:

FEBS Lett. 2017 May ; 591(9): 1247–1257. doi:10.1002/1873-3468.12644.

An essential role of intestinal cell kinase in lung development is linked to the perinatal lethality of human ECO syndrome

Yixin Tong[1,5], **So Hyun Park**[1], **Di Wu**[1], **Wenhao Xu**[2], **Stacey J. Guillot**[2], **Li Jin**[3], **Xudong Li**[3], **Yalin Wang**[4], **Chyuan-Sheng Lin**[6], and **Zheng Fu**[1,*]

[1]Department of Pharmacology, University of Virginia, Charlottesville, VA 22908, USA

[2]Department of Microbiology, Immunology, and Cancer Biology, University of Virginia, Charlottesville, Virginia 22908, USA

[3]Department of Orthopaedic Surgery, University of Virginia, Charlottesville, VA 22908, USA

[4]Department of Cell Biology, University of Virginia, Charlottesville, VA 22908, USA

[5]The Gastrointestinal Surgery Center, Tongji Hospital, Huazhong University of Science & Technology, Hubei, 430030, China

[6]Departments of Pathology and Cell Biology, Columbia University, New York, NY 10032, USA

Abstract

Human endocrine-cerebro-osteodysplasia (ECO) syndrome, caused by the loss-of-function mutation R272Q in the *ICK* (intestinal cell kinase) gene, is a neonatal-lethal developmental disorder. To elucidate the molecular basis of ECO syndrome, we constructed an *Ick* R272Q knock-in mouse model that recapitulates ECO pathological phenotypes. Newborns bearing *Ick* R272Q homozygous mutations die at birth due to respiratory distress. *Ick* mutant lungs exhibit not only impaired branching morphogenesis associated with reduced mesenchymal proliferation, but also significant airspace deficiency in primitive alveoli concomitant with abnormal interstitial mesenchymal differentiation. ICK dysfunction induces elongated primary cilia and perturbs ciliary Hedgehog signaling and autophagy during lung sacculation. Our study identifies an essential role for ICK in lung development and advances the mechanistic understanding of ECO syndrome.

Keywords

intestinal cell kinase (ICK); endocrine-cerebro-osteodysplasia (ECO) syndrome; lung development; primary cilium; Hedgehog signaling; autophagy

*Corresponding author: Zheng Fu, Department of Pharmacology, University of Virginia, PO Box 800735, 1340 Jefferson Park Avenue, Charlottesville, Virginia 22908; Telephone: 434-982-3204; Fax: 434-982-3878; zf6n@virginia.edu.

Author Contributions

ZF and CL conceived and designed the ECO mouse model. YT, SHP, DW, WX, LJ, XL, SJG, YW, ZF performed experiments and conducted data analysis. ZF, CL, WX, XL contributed essential reagents/tools. ZF, YT, SHP contributed to the writing, SJG, CL, WX, LJ, YW contributed to the editing of the manuscript. All authors reviewed the results and approved the final version of the manuscript.

Introduction

Human endocrine-cerebro-osteodysplasia (ECO) syndrome is an autosomal-recessive neonatal-lethal disorder associated with congenital developmental defects in multiple organ systems [1]. A homozygous loss-of-function mutation R272Q in the human *ICK* (intestinal cell kinase) gene, encoding a highly conserved and ubiquitously expressed serine/threonine protein kinase [2, 3], was identified as the causative mutation for ECO [1]. ICK is very similar to MAP kinase in the catalytic domain and contains a MAPK-like TDY motif in its activation loop [3, 4]. By knocking down ICK expression using short-hairpin RNA interference, our work has demonstrated an important role for ICK in the regulation of cell proliferation and survival *in vitro* [5, 6]. An essential role of ICK in human development emerged from the report of human ECO and ECO-like syndromes whose major clinical features include hydrocephalus, polydactyly and micromelia [1, 7, 8]. Recently, *Ick* knockout mouse models revealed similar ECO phenotypes in the cerebral and skeletal systems and linked ICK deficiency to abnormal structure of primary cilium [9, 10]. However, the leading cause of the perinatal lethality phenotype of ECO is still unknown and the underlying cellular and molecular mechanism has not been completely elucidated. To fully understand the structural and mechanistic basis of ECO phenotypes, we generated an *Ick* R272Q knock-in mouse model. The homozygous *Ick* R272Q mutant newborns succumbed to death within minutes of birth due to respiratory distress. Autopsy revealed obvious lung hypoplasia, among other ECO clinical features. Histological analysis indicates an abnormal lung with severe airspace deficiency in alveolar precursors. In this study, we sought to investigate the structural, cellular, and molecular basis underlying lung malfunction in ECO syndrome using the *Ick* R272Q knock-in mouse model.

Materials and methods

Ick^{R272Q} knock-in mouse model for ECO syndrome

The R272Q (CGA>CAA) point mutation was introduced into the exon 8 of the wild-type *Ick* allele on a bacterial artificial chromosome (BAC) to generate *Ick*/R272Q BAC. A LNL (LoxP-Neo-LoxP) cassette was inserted in the intron downstream of exon 8. A gene targeting vector was constructed by retrieving the 5kb long homology arm (5′ to LNL), the LNL cassette, and the 2kb short homology arm (3′ to LNL) into a plasmid vector carrying the DTA (diphtheria toxin alpha chain) negative selection marker. The LNL cassette conferred G418 resistance during gene targeting in PTL1 (129B6 hybrid) ES cells and the DTA cassette provided an autonomous negative selection to reduce the random integration event during gene targeting. Several targeted ES cell clones were identified and injected into C57BL/6 blastocysts to generate chimeric mice. Male chimeras were bred to homozygous EIIa (cre/cre) females (in C57BL/6J background) to excise the neo cassette and to transmit the *Ick*/R272Q allele through germline (Precision Targeting Lab, USA). Ick^{R272Q} heterozygous mice were backcrossed with C57BL/6J for six generations to achieve a complete C57BL/6J genetic background using speed congenic [11]. The R272Q mutation in mouse *Ick* gene was confirmed by genomic DNA sequencing. For timed pregnancy, the presence of a copulation plug in the morning represented embryonic day (E) 0.5. Animal

experiments were carried out according to NIH Animal Welfare Guidelines after approval by the University of Virginia Institutional Animal Care and Use Committee.

Lung histology and morphometric analysis

Whole mouse embryos or isolated lungs were fixed in 4% paraformaldehyde (PFA) for 1–3 days, depending on age and size of the specimen. Fixed embryos or lung tissues were dehydrated through gradient ethanol, placed in xylene and embedded in paraffin. Sections (5 μm) were cut, stained with Hematoxylin and Eosin, and photographed using Olympus BX41 and cellSens imaging software. For morphometric analysis, 20× images of lung sections taken from Aperio ImageScope (Leica Biosystems) were analyzed by ImageJ using the method for quantification of distal air saccular area and mesenchymal thickness as described in [12].

Immunohistochemistry and Western blot

Paraffin sections were immersed in Low pH Flex antigen retrieval solution at 97°C for 20 min, and incubated with Dual Endogenous Enzyme-Block Reagent (Dako) to block endogenous peroxidase and alkaline phosphatase activities. For detection, the peroxidase-based EnVision™+ Dual Link Kit and DAB+ (diaminobenzidine) substrate-chromogen system (Dako) were used. Isolated lungs were snap-frozen in liquid nitrogen and grinded into fine powders on dry-ice. Proteins were extracted from lysed lung tissues, denatured and applied to Western blotting as described in [6]. All commercial antibodies used in the study are listed in Table S1. Scythe phospho-T1080 rabbit antibody was generated in rabbits against phosphopeptides RPL[pT]SPESLSRDLEAC and affinity-purified (Genscript).

Immunofluorescence

Paraffin sections of mouse lung tissues were subjected to antigen retrieval in High pH Target retrieval solution (Dako) before incubation with antibodies. Mouse embryonic fibroblast (MEF) cells were isolated from E14.5–E15.5 embryos and maintained at 37°C and 5% CO_2 in Dulbecco's modified Eagle's medium supplemented with 10% fetal bovine serum, non-essential amino acids, and penicillin-streptomycin using a standard protocol [13]. MEF cells grown on collagen-coated coverslips were fixed by 4% paraformaldehyde (PFA) in PBS, rinsed in PBS, and then permeabilized by 0.2% Triton X-100 in PBS. After one hour in blocking buffer (3% goat serum, 0.2% Triton X-100 in PBS), mouse lung tissue sections or MEF cells on cover slips were incubated with primary antibodies (Table S1) at 4°C overnight followed by rinses in PBS and one hour incubation with Alexa Fluor-conjugated secondary antibodies (Table S1). After extensive rinses, slides were mounted in antifade reagent containing DAPI (4',6-diamidino-2-phenylindole) for imaging (Zeiss AxioImager Z1, Zeiss).

Quantitative RT-PCR

Total RNA was isolated from E18.5 lung tissues and purified using the RNeasy kit (Qiagen) and 1 μg of total RNA was reverse transcribed with oligo-dT primer using iScript cDNA Synthesis Kit (Bio-Rad). Real-time PCR was performed using the Rotor Gene Q instrument

(Qiagen) with KAPA SYBR FAST Universal qPCR Kit (KAPA Bioscience). The primers are listed in Table S2.

Electron microscopy

Lungs were fixed with 2.5% glutaraldehyde and 4% paraformaldehyde in 0.1 M sodium cacodylate buffer at 4°C overnight, and rinsed thoroughly with distilled filtered water. For scanning electron micrographs, the specimens were post-fixed with 2% osmium tetroxide for 30 minutes, rinsed thoroughly with water, dehydrated in a graded ethanol series, dried by a critical point drier, mounted on stubs with silver paint or double-sided conductive carbon stickers, and coated with gold by sputter coater. Lung specimens were examined and photographed using scanning electron microscope (Zeiss Sigma VP HD SEM).

Statistical analysis

Data are presented as means ± SD. Statistical significance was evaluated using a Student's *t*-test, and the P value less than 0.05 was taken as statistically significant.

Results

Construction of the *Ick*^{R272Q} knock-in mouse model for human ECO syndrome

To gain a comprehensive understanding of the cellular and molecular basis underlying developmental phenotypes of ECO syndrome, we generated an ECO mouse model in which the ECO R272Q mutation was "knocked in" the murine *Ick* gene (Fig. 1A). The *Ick* R272Q mutant allele can be distinguished from the wild type allele based on the size of a PCR product within the knocked-in region that is congenic with the R272Q mutation (Fig. 1A–B). The "knocked in" mutation R272Q in the mouse *Ick* gene was confirmed by genomic DNA sequencing (Fig. 1C). Inhibitory effect of the R272Q mutation on ICK catalytic activity was confirmed by assessing phosphorylation of its substrate Scythe [14] (Fig. 1L). Mice heterozygous for the targeted allele ($Ick^{R272Q/+}$) were phenotypically normal.

Ick^{R272Q} homozygous mice died shortly after birth due to respiratory failure

$Ick^{R272Q/+}$ heterozygous mice were interbred to produce $Ick^{R272Q/R272Q}$ homozygous mice. Among a total of 292 embryos harvested at E12.5–E18.5, 24% were wild type, 48% were heterozygous, and 28% were homozygous (Table S3). Among a total of 122 heterozygous intercross offspring genotyped at birth or 3 weeks postpartum, 30% were wild type, 48% were heterozygous, and no live R272Q homozygous mice were found (Table S4). In all cases, pups that showed severe gasping and died within minutes of birth were genotyped as the R272Q homozygous mutants that displayed essential ECO pathological features such as polydactyly and shortened limbs (Fig. S1). Inadequate oxygenation of the blood in R272Q homozygous mutant lungs was evident (Fig. 1D). These results indicate that $Ick^{R272Q/R272Q}$ knock-in mouse model can phenotypically replicate human ECO syndrome and impaired transition to air breathing at birth may significantly contribute to the cause of ECO perinatal lethality.

Ick^{R272Q} homozygous mutant lungs displayed significant airspace deficiency but normal differentiation of alveolar epithelial cells in primitive alveoli

Ick^{R272Q} homozygous lungs had the normal shape, number and arrangement of lobes but were hypoplastic and severely deficient in airspace (Fig. 1D, Fig. S2G–H). Morphometric analyses of *Ick*^{R272Q} homozygous lungs further indicate a significant reduction in lung saccular area and a marked increase in mesenchymal thickness (Fig. 1E, Fig. S2I). The formation of alveolar precursors was severely disrupted as a result of deficient ICK signaling (Fig. 1 and Fig. S2). Alveolar type 1 (AT1) and type 2 (AT2) epithelial cells are essential building units of alveoli. *Ick*$^{R272Q/R272Q}$ mutant lungs expressed the AT1 marker podoplanin (PDPN) and the AT2 marker surfactant protein C (SFTPC) at normal levels and in a pattern similar to that of wild type or *Ick*$^{R272Q/+}$ littermates (Fig. 1F–K). Electron micrographs confirmed that *Ick* mutant lungs had both AT1 and AT2 cells as well as secreted surfactants in airspace (Fig. S3A–B), which is consistent with the presence of lamellar bodies and glycogen particles in *Ick* mutant AT2 cells (Fig. S3C). These observations suggest that ICK function is not essential for the differentiation of alveolar epithelial cells and that airspace deficiency in *Ick* mutant lungs are not caused by the lack of AT1 and AT2 cells or a deficiency in secreted surfactants.

Defective ICK signaling reduced lung branching associated with decreased mesenchymal cell proliferation during morphogenesis

To evaluate branching at the pseudoglandular stage (E11.5–16.5), whole-mount lungs were isolated from E12.5–E13.5 embryos. The number of lung buds (branching points) per area was reduced by about 50% in *Ick* mutant lungs as compared with normal littermate controls (Fig. 2A–C), suggesting that lung branching morphogenesis is compromised in *Ick* mutant lungs. The bronchial tree develops through extensive proliferation of distal epithelium and surrounding mesenchyme. Proliferation of the distal lung epithelium and mesenchyme at E12.5 was examined by immunohistochemistry using Ki67 and phospho-Histone H3 as proliferation markers (Fig. 2D–E, Fig. S4A–B). *Ick* mutant lungs showed a significant decrease in the number of proliferating mesenchymal but not epithelial cells (Fig. 2F), suggesting that impaired mesenchymal cell proliferation may cause reduced lung branching in ECO syndrome.

An excess of smooth muscle actin (SMA)-positive mesenchymal cells were present in the thickened interstitium of *Ick*^{R272Q} homozygous mutant lungs

During alveolar development at the saccular stage (E16.5–18.5), in addition to the differentiation of the two main specialized epithelial cell types of the future alveolus, a major morphogenetic event that occurs is the thinning and remodeling of lung interstitium, a process that is still mechanistically poorly understood. Compared with wild type lungs, *Ick* mutant lungs displayed excessive cellularity in the interstitium (Fig. 1, Fig. S2), suggesting the thinning process is blocked. Given the abundance of proliferating cells in *Ick* mutant lungs was not significantly different from that of wild type lungs at E18.5 (Fig. S5), over-proliferation is not the primary cause of the interstitial hypercellularity in *Ick* mutant lungs. Apoptosis may contribute to the thinning of interstitium between airspaces and the formation of air saccules [15]. However, assessing cell death in *Ick* wild type versus R272Q mutant

lungs was experimentally difficult because of the low number of cells undergoing this process in the normal lung, as reported in [16] and confirmed in our study. Therefore, although no significant difference in the percentage of labelled apoptotic cells (0.04–0.05%) was observed between *Ick* R272Q homozygous mutant and littermate normal lungs during interstitium remodeling (unpublished data), we cannot completely exclude the possible contribution of aberrant cell apoptosis to the interstitial hypercellularity in *Ick* mutant lungs.

Intriguingly, Western blot analysis revealed that *Ick* mutant lungs expressed a significantly increased amount of smooth muscle actin (SMA) but a similar amount of epithelial cell marker E-cadherin (CDH1) and AT2 cell marker SFTPC when compared with wild type lungs (Fig. 3C). Immunohistochemistry confirmed the presence of an excessive number of SMA-positive mesenchymal cells in the interstitium of *Ick* mutant lungs (Fig. 3A–B, A′–B′). In contrast, the expression pattern of SMA-positive smooth muscle cells in pulmonary vessels and bronchioli of *Ick* mutant lungs was very similar to that of normal lungs (Fig. S6). These results suggest that an accumulation of SMA-positive mesenchymal cells in the interstitium may contribute to the impaired thinning of interstitium.

The TGFβ/Smad signaling pathway is a major transcription-regulating mechanism for α-SMA expression. Compared with normal lungs, *Ick* mutant lungs did not display any significant changes in the expression levels of Smad2 and Smad3 (Fig. 3C). Furthermore, TGFβ receptor complex-activated phosphorylation of Smad2 and Smad3 was not elevated, instead a moderate decrease in phospho-Smad2 signals was observed in *Ick* mutant lungs (Fig. 3C). This result suggests that a Smad signaling-independent mechanism underlies the increased expression of α-SMA in *Ick* mutant lungs.

Loss of ICK function induced elongated primary cilia in embryonic lungs

ICK has an evolutionarily conserved role in the structural maintenance of primary cilium through regulation of intraflagellar transport (IFT) [10, 17, 18]. Recently, ICK localization was reported on primary cilia of mammalian cells [7, 9, 10, 18–20]. Using the primary cilium marker Arl13B (Fig. 4A, B), we sought to determine whether loss of ICK function impairs ciliary structure during embryonic lung development. Quantitative analyses indicate that deficient ICK signaling induced a significant increase in the length of primary cilium in the developing lung (Fig. 4C). A similar phenotype in ciliary length was observed in $Ick^{R272Q/R272Q}$ lungs through scanning electron microscopy (Fig. 4D). Using molecular markers for primary cilium (acetylated tubulin and Arl13B), we also showed that loss of ICK function induced elongation of primary cilium in mouse embryonic fibroblast (MEF) cells (Fig. 4E–M).

ICK dysfunction altered Sonic hedgehog signaling and autophagy status

Primary cilia are not only sensory organelles but also signaling hubs linked to Sonic Hedgehog (Shh) signaling during vertebrate development. *Ick* mutant lungs (E18.5) exhibited increased expression of genes that are essential for Shh signaling such as *Shh* ligands, Shh transmembrane receptor *Patched2* (*Ptch2*), transmembrane regulator *Smoothened* (*Smo*), and transcription activator *Gli2* as well as decreased expression of a vertebrate Hh-specific inhibitor, *Hedgehog interacting protein* (*Hhip*) (Fig. 5E).

Immunohistochemistry confirmed up-regulated expression of Gli2 and Ptch2 proteins in a subset of cells in E18.5 *Ick* mutant lungs (Fig. 5A–D). These results indicate that disrupting ICK signaling in E18.5 embryonic lungs induced an upregulation of Shh signaling associated with elongated primary cilia.

Given the reciprocal regulations of primary cilium and autophagy [21], we assessed the basal autophagy status in E18.5 *Ick* wild type and mutant lungs by analyzing the expression levels of two autophagy markers: LC3 (microtubule-associated protein light chain 3) and SQSTM1 (sequestosome 1). LC3 was detected as two bands on immunoblot: cytosolic LC3-I (upper band) and membrane-associated LC3-II (lower band). LC3-II is specifically localized on autophagosomes, and its level correlates with autophagic vesicle numbers [22, 23]. SQSTM1 binds LC3 and serves as a selective substrate for autophagy [24]. Inhibition of autophagy correlates with increased levels of SQSTM1 whereas decreased levels of SQSTM1 are associated with autophagy induction, suggesting that steady-state levels of SQSTM1 reflect the autophagic status [25, 26]. An increase in LC3-II signals concurrent with a marked decrease in SQSTM1 signals were detected in *Ick* R272 homozygous mutant lungs as compared with either wild type or R272 heterozygous mutant lungs (Fig. 5F). This result suggests that deficient ICK signaling in the lung elicited an increase in basal autophagy. To further examine whether ICK regulates the activity of the autophagy pathway, we used MEFs to evaluate the autophagy flux and its degradative activity. Under the steady-state, *Ick* mutant MEFs exhibited less LC3 and SQSTM1 signals than wild type MEFs (Fig. 5G). Upon induction of autophagy by starvation, LC3 and SQSTM1 signals in wild type cells were significantly reduced to the levels of *Ick* mutant cells prior to starvation (Fig. 5G). In both the steady-state and starvation conditions, *Ick* mutant cells displayed significantly less LC3 and SQSTM1 signals than wild type cells, indicating a faster autophagy flux and quicker degradative process in *Ick* mutant cells. Taken together, our results suggest that the autophagy status is significantly altered by ICK dysfunction.

Discussion

Our studies have established ICK as an essential molecular determinant of lung development and provided new mechanistic insights into the perinatal lethality phenotype of human ECO syndrome. Although recent studies from *Ick* knockout mouse models linked ICK deficiency to defective ciliary structure and transport in the neuronal and skeletal systems, it was not clear how this link affects any specific cellular processes during embryonic development that cause the perinatal death in ECO patients. Using an ECO mouse model, we report here that ICK dysfunction can lead to an abnormal lung with severe alveolar airspace deficiency and respiratory failure at birth. Mesenchymal cell proliferation during lung branching morphogenesis and interstitial mesenchymal cell differentiation and remodeling during lung sacculation are two important cellular mechanisms by which ICK regulates embryonic lung development. Loss of ICK function perturbed not only ciliary structure and Hedgehog signaling but also autophagy, a highly conserved intracellular process in the maintenance of cell homeostasis.

The dependence of Hedgehog (Hh) signaling on the integrity of a primary cilium has been well established. Even though in *Ick* null cells opposite effects on ciliary length were

observed in neural tubes (shortened) and limb buds (elongated), abnormal ciliary localization and expression of Hh pathway components is associated with compromised Hh signaling in both cases, albeit with different patterns. In one case, decreased expression of Hh-targeted genes *Gli1* and *Ptch1* was observed in the posterior region of limb buds [9]. In the other case, Gli2 and Gli3 signals were enriched at cilia tips in *Ick* null cells even without Hh pathway stimulation, and ciliary Smo signals were increased in *Ick* null neural tubes [10]. In *Ick* R272Q mutant embryonic lungs, significant alterations in Hh-targeted genes such as *Gli2* and *Ptch2* were observed at E18.5, the saccular stage (Fig. 5E), but not at E14.5, the pseudoglandular stage (Fig. S7). These results suggest that the effect of impaired ciliary structure induced by loss of ICK function on Hh signaling may depend on not only specific tissue and cellular contexts but also specific developmental stages. The selective effects of deficient ICK signaling on *Gli2* and *Ptch2*, but not *Gli1* and *Ptch1*, in E18.5 *Ick* mutant lungs are also intriguing. *Gli2*, but not *Gli1*, is primarily required for activation of Hh signaling [27]. Ectopic overexpression of GLI2 can drive increased expression of *Shh*, *Ptch1*, *Ptch2*, *Smo*, *Hhip*, and *Gli1* in the developing mouse lung [28]. Despite the strong correlative evidence from *Ick* knockout and *Ick* R272Q mutant mouse models, further studies are required to establish a functional relationship between Hh signaling and the ECO phenotypes and elucidate the mechanisms underlying the tissue context- and developmental stage-dependent selective effects of ICK on the Hh signaling.

Our data here provided further evidence underscoring the importance of Sonic hedgehog (Shh) signaling in lung development and disease [29]. There are significant similarities between the phenotypes of *Ick* R272Q mutant lungs and transgenic lungs overexpressing Shh [16]. Both *Shh* transgenic and *Ick* R272Q mutant newborns died soon after birth due to respiratory failure linked to the absence of functional alveoli. Either Shh overexpression or ICK dysfunction resulted in an abnormal lung showing extensive mesenchyme between undilated air saccules but normal differentiation of alveolar epithelial cells. This excess mesenchyme probably interferes with sacculation and the formation of functional alveoli, but the underlying mechanisms may be different. In *Shh* transgenic lungs, increased mesenchymal proliferation may contribute primarily to the excessive interstitial mesenchyme [16]. In *Ick* mutant lungs, no significant increase in cell proliferation at the saccular stage was detected. The thickened interstitial mesenchyme of *Ick* mutant lungs has an overabundance of SMA-positive cells, suggesting that abnormal mesenchymal differentiation may impair interstitial remodeling and disrupt sacculation.

Previously we identified Scythe as an ICK interacting protein and candidate substrate from a yeast two-hybrid screening [14]. In mammalian cells, ICK directly interacts with Scythe and phosphorylates Scythe *in vitro* at Thr-1080 [14]. Our new data showing ICK phosphorylation of Scythe Thr-1080 *in vivo* (Fig. 1) strongly suggest that Scythe is an ICK substrate to mediate its downstream signaling events in the developing lung. Scythe is a co-chaperone protein with diverse regulatory functions in protein biogenesis and degradation [30]. Gene-targeted deletion of Scythe in mice resulted in perinatal lethality associated with ECO-like lung phenotypes [31]. Autophagy was also impaired in lungs of *Scythe* null mouse embryos [32]. Autophagy has been implicated in playing a critical role of facilitating the thinning of the alveolar septa that is necessary for effective gas exchange during the transition to air breathing at birth [33]. Further investigation is required to determine

whether abnormal autophagy due to disruption of the ICK-scythe signaling axis can lead to impaired thinning of lung interstitial mesenchyme and malformation of alveoli in ECO syndrome. Several lines of evidences from previous studies suggest that ciliogenesis and autophagy are intricately linked and reciprocally regulated [34–36]. A major goal of our future studies is to address whether ICK directly targets autophagy first to regulate ciliogenesis and Hh signaling or vice versa in the determination of cell fate and phenotype.

Supplementary Material

Refer to Web version on PubMed Central for supplementary material.

Acknowledgments

We thank our colleagues at UVA Research Histology, Biorepository and Tissue Research Facility, Advanced Microscopy, and DNA Sciences for excellent technical support, and Dr. Ruth Stornetta for technical guidance in immunofluorescence microscopy and imaging. This work was partially supported by National Institute of Health grants DK082614 and CA195273 to Z.F.

Abbreviations

ICK	intestinal cell kinase
ECO	endocrine-cerebral-osteodysplasia
SHH	Sonic Hedgehog
Gli	glioma-associated oncogene
AT1/AT2	alveolar type 1/type 2 epithelial cell
PDPN	podoplanin
SFTPC	surfactant protein C
SMA	smooth muscle actin
LC3	microtubule-associated protein light chain 3
SQSTM1	sequestosome 1
CDH1	cell adhesion molecule 1/E-cadherin
MEF	mouse embryonic fibroblast

References

1. Lahiry P, Wang J, Robinson JF, Turowec JP, Litchfield DW, Lanktree MB, Gloor GB, Puffenberger EG, Strauss KA, Martens MB, et al. A multiplex human syndrome implicates a key role for intestinal cell kinase in development of central nervous, skeletal, and endocrine systems. Am J Hum Genet. 2009; 84:134–147. [PubMed: 19185282]
2. Abe S, Yagi T, Ishiyama S, Hiroe M, Marumo F, Ikawa Y. Molecular cloning of a novel serine/threonine kinase, MRK, possibly involved in cardiac development. Oncogene. 1995; 11:2187–2195. [PubMed: 8570168]

3. Togawa K, Yan YX, Inomoto T, Slaugenhaupt S, Rustgi AK. Intestinal cell kinase (ICK) localizes to the crypt region and requires a dual phosphorylation site found in map kinases. J Cell Physiol. 2000; 183:129–139. [PubMed: 10699974]

4. Fu Z, Schroeder MJ, Shabanowitz J, Kaldis P, Togawa K, Rustgi AK, Hunt DF, Sturgill TW. Activation of a nuclear Cdc2-related kinase within a mitogen-activated protein kinase-like TDY motif by autophosphorylation and cyclin-dependent protein kinase-activating kinase. Mol Cell Biol. 2005; 25:6047–6064. [PubMed: 15988018]

5. Fu Z, Kim J, Vidrich A, Sturgill TW, Cohn SM. Intestinal cell kinase, a MAP kinase-related kinase, regulates proliferation and G1 cell cycle progression of intestinal epithelial cells. Am J Physiol Gastrointest Liver Physiol. 2009; 297:G632–640. [PubMed: 19696144]

6. Bolick DT, Chen T, LA OA, Tong Y, Wu D, Joyner LT 2nd, Oria RB, Guerrant RL, Fu Z. Intestinal cell kinase is a novel participant in intestinal cell signaling responses to protein malnutrition. PLoS One. 2014; 9:e106902. [PubMed: 25184386]

7. Oud MM, Bonnard C, Mans DA, Altunoglu U, Tohari S, Ng AY, Eskin A, Lee H, Rupar CA, de Wagenaar NP, et al. A novel ICK mutation causes ciliary disruption and lethal endocrine-cerebro-osteodysplasia syndrome. Cilia. 2016; 5:8. [PubMed: 27069622]

8. Paige Taylor S, Kunova Bosakova M, Varecha M, Balek L, Barta T, Trantirek L, Jelinkova I, Duran I, Vesela I, Forlenza KN, et al. An inactivating mutation in intestinal cell kinase, ICK, impairs hedgehog signalling and causes short rib-polydactyly syndrome. Hum Mol Genet. 2016

9. Moon H, Song J, Shin JO, Lee H, Kim HK, Eggenschwiller JT, Bok J, Ko HW. Intestinal cell kinase, a protein associated with endocrine-cerebro-osteodysplasia syndrome, is a key regulator of cilia length and Hedgehog signaling. Proc Natl Acad Sci U S A. 2014; 111:8541–8546. [PubMed: 24853502]

10. Chaya T, Omori Y, Kuwahara R, Furukawa T. ICK is essential for cell type-specific ciliogenesis and the regulation of ciliary transport. EMBO J. 2014; 33:1227–1242. [PubMed: 24797473]

11. Wakeland E, Morel L, Achey K, Yui M, Longmate J. Speed congenics: a classic technique in the fast lane (relatively speaking). Immunol Today. 1997; 18:472–477. [PubMed: 9357138]

12. Wang Y, Frank DB, Morley MP, Zhou S, Wang X, Lu MM, Lazar MA, Morrisey EE. HDAC3-Dependent Epigenetic Pathway Controls Lung Alveolar Epithelial Cell Remodeling and Spreading via miR-17–92 and TGF-beta Signaling Regulation. Dev Cell. 2016; 36:303–315. [PubMed: 26832331]

13. Durkin ME, Qian X, Popescu NC, Lowy DR. Isolation of Mouse Embryo Fibroblasts. Bio Protoc. 2013; 3

14. Fu Z, Larson KA, Chitta RK, Parker SA, Turk BE, Lawrence MW, Kaldis P, Galaktionov K, Cohn SM, Shabanowitz J, et al. Identification of yin-yang regulators and a phosphorylation consensus for male germ cell-associated kinase (MAK)-related kinase. Mol Cell Biol. 2006; 26:8639–8654. [PubMed: 16954377]

15. Del Riccio V, van Tuyl M, Post M. Apoptosis in lung development and neonatal lung injury. Pediatr Res. 2004; 55:183–189. [PubMed: 14630991]

16. Bellusci S, Furuta Y, Rush MG, Henderson R, Winnier G, Hogan BL. Involvement of Sonic hedgehog (Shh) in mouse embryonic lung growth and morphogenesis. Development. 1997; 124:53–63. [PubMed: 9006067]

17. Burghoorn J, Dekkers MP, Rademakers S, de Jong T, Willemsen R, Jansen G. Mutation of the MAP kinase DYF-5 affects docking and undocking of kinesin-2 motors and reduces their speed in the cilia of Caenorhabditis elegans. Proc Natl Acad Sci U S A. 2007; 104:7157–7162. [PubMed: 17420466]

18. Broekhuis JR, Verhey KJ, Jansen G. Regulation of cilium length and intraflagellar transport by the RCK-kinases ICK and MOK in renal epithelial cells. PLoS One. 2014; 9:e108470. [PubMed: 25243405]

19. Yang Y, Roine N, Makela TP. CCRK depletion inhibits glioblastoma cell proliferation in a cilium-dependent manner. EMBO Rep. 2013; 14:741–747. [PubMed: 23743448]

20. Paige Taylor S, Kunova Bosakova M, Varecha M, Balek L, Barta T, Trantirek L, Jelinkova I, Duran I, Vesela I, Forlenza KN, et al. An inactivating mutation in intestinal cell kinase, ICK, impairs

hedgehog signalling and causes short rib-polydactyly syndrome. Hum Mol Genet. 2016; 25:3998–4011. [PubMed: 27466187]

21. Pampliega O, Cuervo AM. Autophagy and primary cilia: dual interplay. Curr Opin Cell Biol. 2016; 39:1–7. [PubMed: 26826446]
22. Kabeya Y, Mizushima N, Ueno T, Yamamoto A, Kirisako T, Noda T, Kominami E, Ohsumi Y, Yoshimori T. LC3, a mammalian homologue of yeast Apg8p, is localized in autophagosome membranes after processing. EMBO J. 2000; 19:5720–5728. [PubMed: 11060023]
23. Xie Z, Klionsky DJ. Autophagosome formation: core machinery and adaptations. Nat Cell Biol. 2007; 9:1102–1109. [PubMed: 17909521]
24. Pankiv S, Clausen TH, Lamark T, Brech A, Bruun JA, Outzen H, Overvatn A, Bjorkoy G, Johansen T. p62/SQSTM1 binds directly to Atg8/LC3 to facilitate degradation of ubiquitinated protein aggregates by autophagy. J Biol Chem. 2007; 282:24131–24145. [PubMed: 17580304]
25. Komatsu M, Wang QJ, Holstein GR, Friedrich VL Jr, Iwata J, Kominami E, Chait BT, Tanaka K, Yue Z. Essential role for autophagy protein Atg7 in the maintenance of axonal homeostasis and the prevention of axonal degeneration. Proc Natl Acad Sci U S A. 2007; 104:14489–14494. [PubMed: 17726112]
26. Wang QJ, Ding Y, Kohtz DS, Mizushima N, Cristea IM, Rout MP, Chait BT, Zhong Y, Heintz N, Yue Z. Induction of autophagy in axonal dystrophy and degeneration. J Neurosci. 2006; 26:8057–8068. [PubMed: 16885219]
27. Bai CB, Auerbach W, Lee JS, Stephen D, Joyner AL. Gli2, but not Gli1, is required for initial Shh signaling and ectopic activation of the Shh pathway. Development. 2002; 129:4753–4761. [PubMed: 12361967]
28. Rutter M, Wang J, Huang Z, Kuliszewski M, Post M. Gli2 influences proliferation in the developing lung through regulation of cyclin expression. Am J Respir Cell Mol Biol. 2010; 42:615–625. [PubMed: 19574535]
29. Kugler MC, Joyner AL, Loomis CA, Munger JS. Sonic hedgehog signaling in the lung. From development to disease. Am J Respir Cell Mol Biol. 2015; 52:1–13. [PubMed: 25068457]
30. Lee JG, Ye Y. Bag6/Bat3/Scythe: a novel chaperone activity with diverse regulatory functions in protein biogenesis and degradation. Bioessays. 2013; 35:377–385. [PubMed: 23417671]
31. Desmots F, Russell HR, Lee Y, Boyd K, McKinnon PJ. The reaper-binding protein scythe modulates apoptosis and proliferation during mammalian development. Mol Cell Biol. 2005; 25:10329–10337. [PubMed: 16287848]
32. Sebti S, Prebois C, Perez-Gracia E, Bauvy C, Desmots F, Pirot N, Gongora C, Bach AS, Hubberstey AV, Palissot V, et al. BAT3 modulates p300-dependent acetylation of p53 and autophagy-related protein 7 (ATG7) during autophagy. Proc Natl Acad Sci U S A. 2014; 111:4115–4120. [PubMed: 24591579]
33. Cheong H, Wu J, Gonzales LK, Guttentag SH, Thompson CB, Lindsten T. Analysis of a lung defect in autophagy-deficient mouse strains. Autophagy. 2014; 10:45–56. [PubMed: 24275123]
34. Tang Z, Lin MG, Stowe TR, Chen S, Zhu M, Stearns T, Franco B, Zhong Q. Autophagy promotes primary ciliogenesis by removing OFD1 from centriolar satellites. Nature. 2013; 502:254–257. [PubMed: 24089205]
35. Wang S, Livingston MJ, Su Y, Dong Z. Reciprocal regulation of cilia and autophagy via the MTOR and proteasome pathways. Autophagy. 2015; 11:607–616. [PubMed: 25906314]
36. Pampliega O, Orhon I, Patel B, Sridhar S, Diaz-Carretero A, Beau I, Codogno P, Satir BH, Satir P, Cuervo AM. Functional interaction between autophagy and ciliogenesis. Nature. 2013; 502:194–200. [PubMed: 24089209]

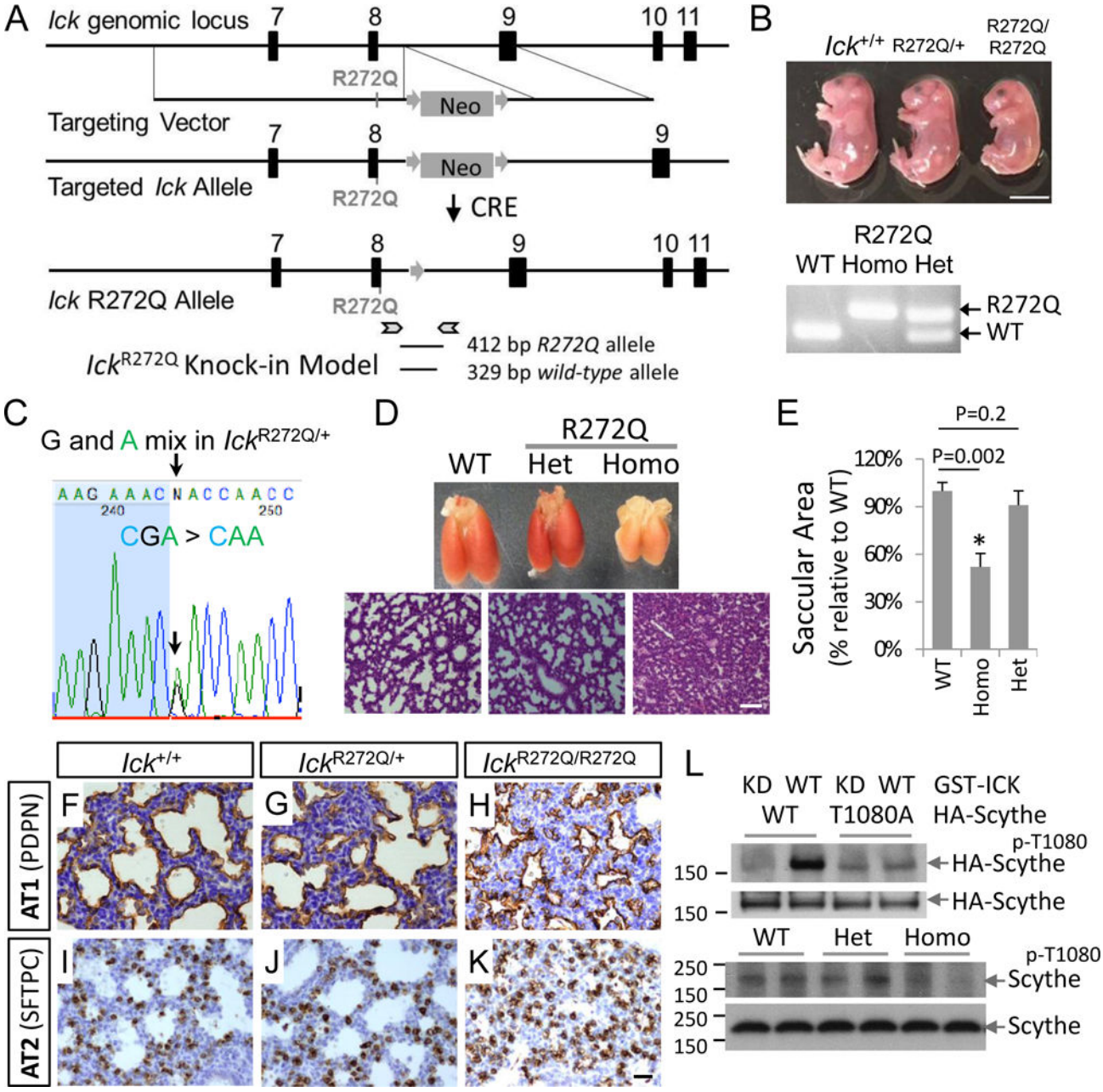

Fig. 1.

Ick R272Q knock-in mouse model for human ECO syndrome displayed a hypoplastic lung with abnormal air saccular structures. (A) Diagram of the targeting strategy used to generate the *Ick* R272Q knock-in allele and the genotyping strategy used to determine the wild-type and the targeted *Ick* alleles. (B) E18.5 embryos of three genotypes based on tail DNA PCR results. Scale bar, 1cm. (C) Genomic DNA sequencing data confirming the presence of the R272Q mutation in mouse *Ick* gene. (D) Gross view of neonatal lungs at P0 and Hematoxylin & Eosin-stained lung tissue sections. Scale bar, 100 μm. (E) Quantification of lung saccular areas in E18.5 lungs (Mean ± SD, n=4, *P<0.01). (F–K) E18.5 lung tissue sections immuno-stained with alveolar type 1 and type 2 cell markers. Scale bar, 20 μm. (L)

Assessing the ICK catalytic activity using its specific *in vivo* target, the phospho-Scythe^{T1080} signal. Top blot: GST-ICK wild type (WT) or kinase dead (KD) and HA-Scythe wild type (WT) or T1080A mutant were co-expressed in HEK293T cells. HA-Scythe was purified and analyzed for p-Scythe^{T1080} signal. Bottom blot: Equal amount of total proteins extracted from E18.5 lungs were blotted for p-T1080 specific and total Scythe signals.

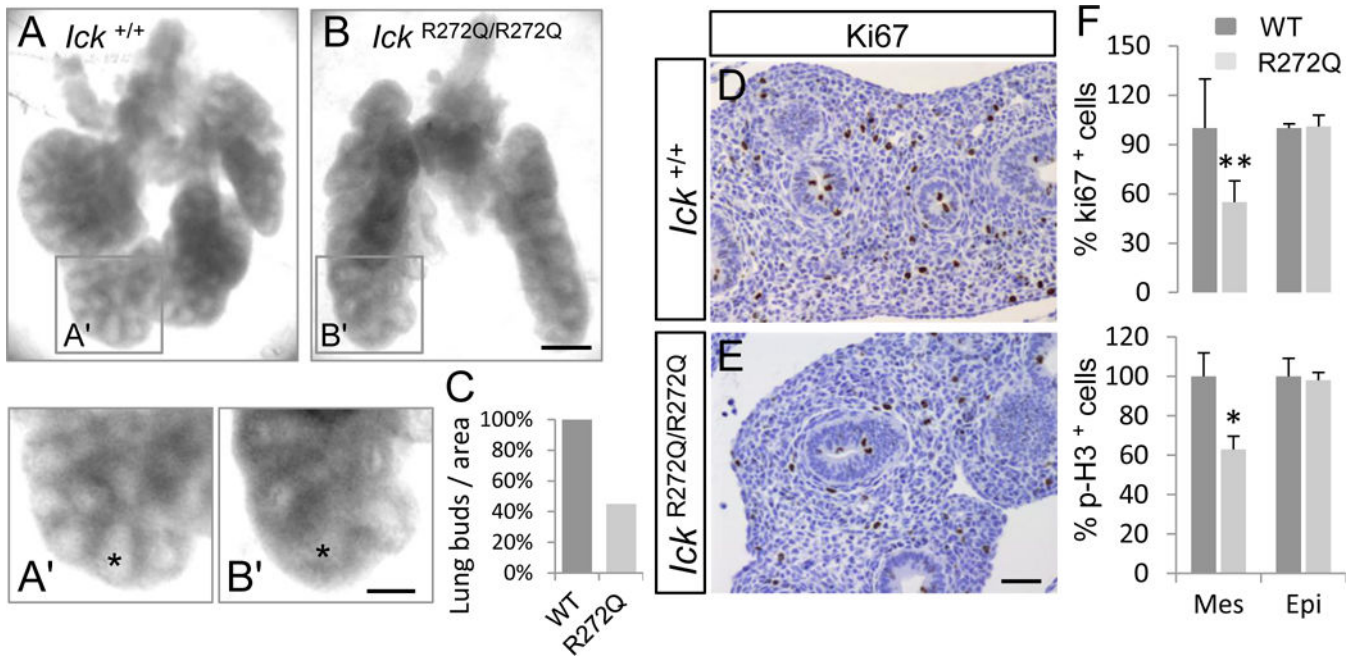

Fig. 2.

Ick$^{R272Q/R272Q}$ mutant lung exhibited impaired branching associated with reduced distal mesenchymal proliferation. (A–B) Whole-mount lungs isolated from E13.5 embryos. (A'–B') Blow-up images illustrating lung buds, as denoted by the asterisk symbol. (C) Quantification of the number of lung buds per area indicates about 50% reduction in the number of branching points in *Ick* mutant lungs. Shown are representative images and data from five pairs of E12.5–13.5 wild type and *Ick* mutant lungs. Scare bars: 500 μm (A–B), 250 μm (A'–B'). (D–E) E12.5 lung tissue sections immuno-stained with proliferation marker Ki67. Scale bar, 50 μm. (F) Quantification of Ki67 and phospho-Histone H3 positive cells in E12.5 lung epithelium and mesenchyme indicates a significant decrease in the number of proliferating mesenchymal cells in *Ick* mutant lungs during branching morphogenesis (Mean ± SD, n=3, *P<0.05, **P<0.01).

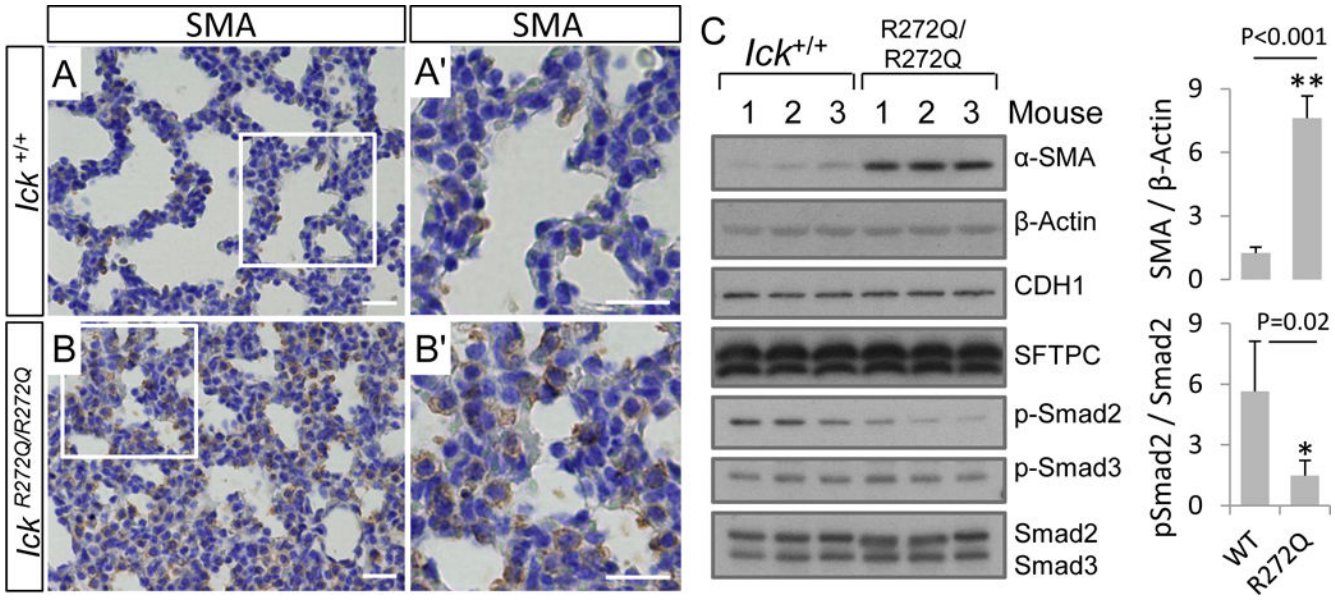

Fig. 3.

Ick$^{R272Q/R272Q}$ mutant lung displayed an excessive amount of smooth muscle actin (SMA)-positive mesenchymal cells in the hypercellular interstitium. (A–B) E18.5 lung tissue sections immuno-stained for α-smooth muscle actin (α-SMA). (A´–B´) High magnification images showing an excess of SMA-positive cells in *Ick* mutant lung interstitium. Scale bars, 20 μm. (C) Western blots of α-SMA, E-cadherin (CDH1), β-Actin, SFTPC, total and phospho-Smad2/3 signals in E18.5 lung tissue extracts. Quantification data of α-SMA signals against β-Actin and phospho-Smad2 against total Smad2 indicate up-regulated expression of α-SMA proteins and down-regulated phospho-Smad2 signals in *Ick* mutant lungs (Mean ± SD, n=6, *P<0.01, **P<0.001).

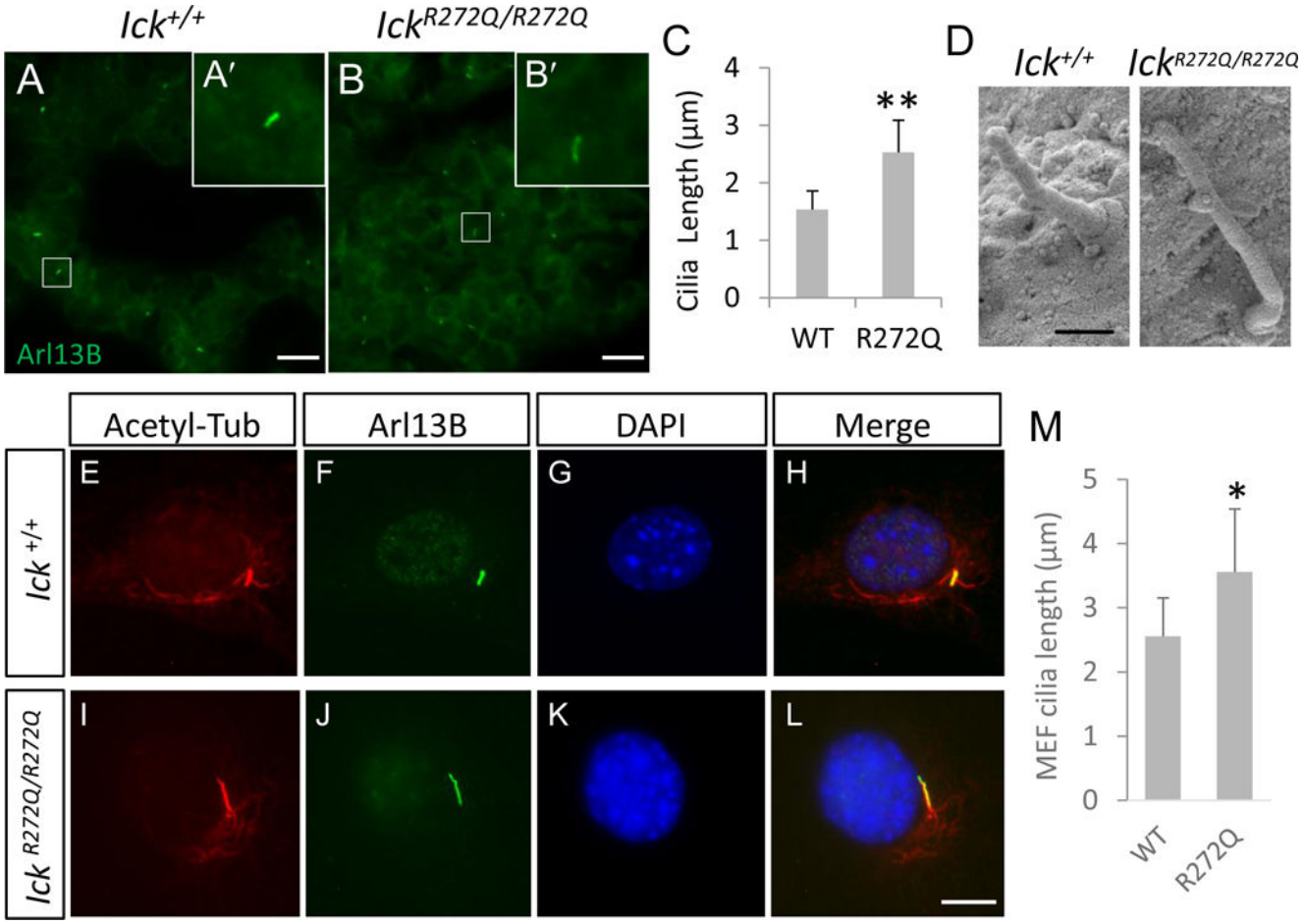

Fig. 4.

Loss of ICK function induced elongated primary cilia. (A, B) Lung tissue sections from *Ick*$^{+/+}$ and *Ick*$^{R272Q/R272Q}$ E18.5 embryos stained for the primary cilium marker Arl13B. (A ´, B´) Blow up images of a primary cilium. Scale bar, 10 μm. (C) Ciliary length in E18.5 *Ick*$^{R272Q/R272Q}$ mutant (2.53 ± 0.55 μm, n=64 cilia) and *Ick*$^{+/+}$ wild type (1.53 ± 0.32 μm, n=87 cilia) lungs were measured using Image J. **P<0.001. (D) Representative scanning electron micrographs showing elongated primary cilium in E18.5 *Ick* $^{R272Q/R272Q}$ mutant lung. Scale bar, 500 nm. (E–L) Immunofluorescence images of primary cilium marker (Acetylated tubulin and Arl13B) staining on mouse embryonic fibroblast (MEF) cells isolated from *Ick* mutant and wild type littermate embryos. Scale bar, 50 μm. (M) Ciliary length in *Ick*$^{R272Q/R272Q}$ mutant MEF cells (3.56 ± 0.97 μm, n=30 cells) and wild type MEF cells (2.55 ± 0.6 μm, n=30 cells) were measured using Image J. *P < 0.01.

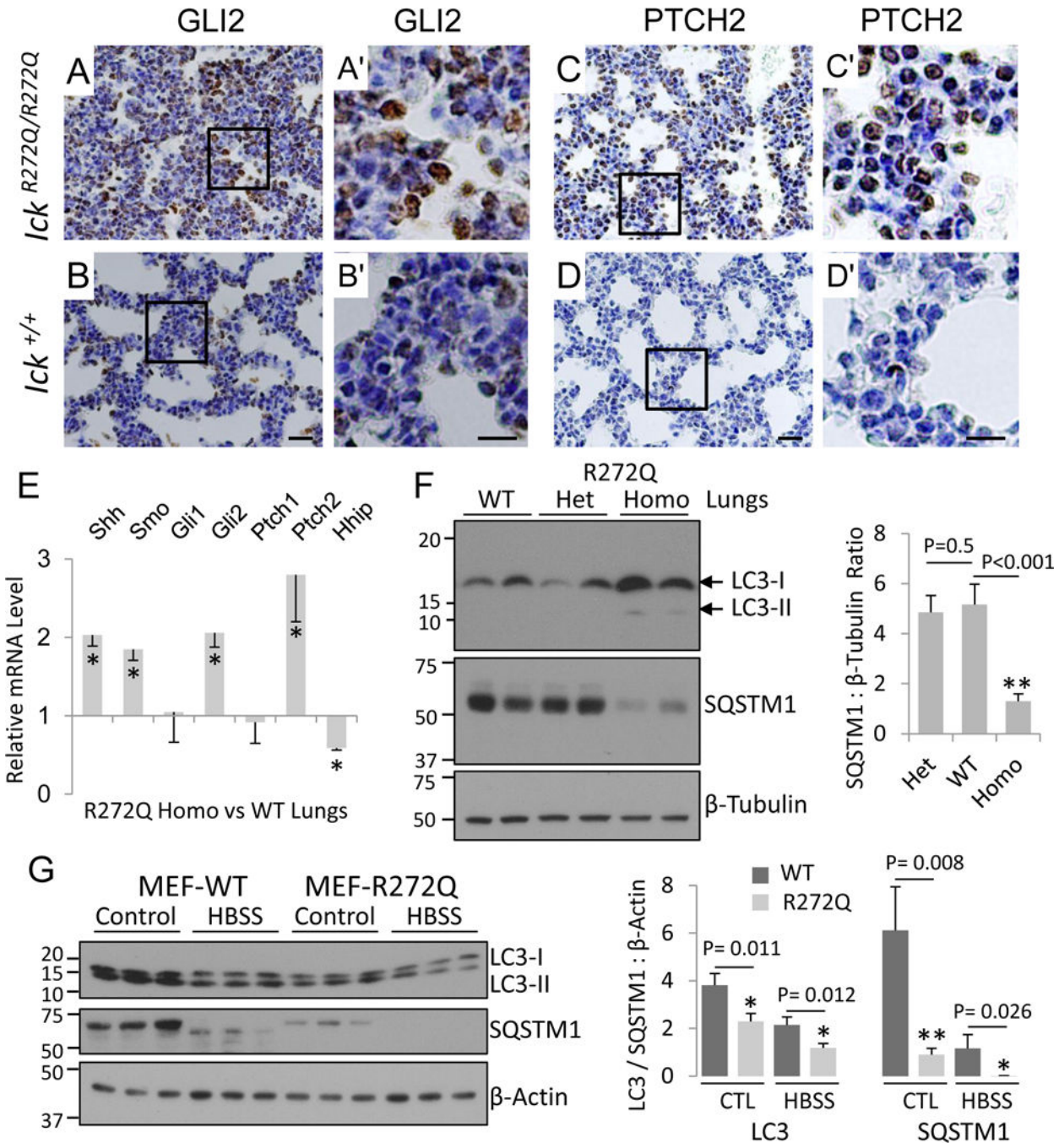

Fig. 5.

ICK dysfunction altered ciliary Hedgehog signaling and autophagy. (A–D) E18.5 lung tissue sections immuno-stained for Gli2 and Ptch2. (A´–D´) High magnification images showing elevated expression of Gli2 and Ptch2 in a subset of cells in *Ick* R272Q homozygous mutant lungs. Scale bars: 20 μm (A–D), 10 μm (A´–D´). (E) Relative mRNA levels of the Sonic Hedgehog pathway components in E18.5 *Ick* R272Q homozygous mutant versus wild type lungs (Mean ± SD, n=6, *P<0.05). (F) Western blots of autophagy markers LC3 and SQSTM1 in E18.5 lung tissue extracts. Quantification of SQSTM1 against β-Tubulin signals

indicates a significant decrease in SQSTM1 signals in *Ick* R272Q homozygous mutant lungs (Mean ± SD, n=6, **P<0.001). (G) Western blots of autophagy markers LC3 and SQSTM1 in mouse embryonic fibroblasts (MEFs) grown in either normal medium (control) or starved in Hank's Balanced Salt Solution (HBSS) for 2 hours. Quantification of LC3 and SQSTM1 against β-Actin signals indicates a significant decrease in autophagy markers in *Ick* R272Q homozygous mutant MEFs under the steady-state or starvation-induced autophagic flux (Mean ± SD, n=3, *P<0.05, **P<0.01).